NeuroImage: Clinical 15 (2017) 832–842

Contents lists available at ScienceDirect

NeuroImage: Clinical

journal homepage: www.elsevier.com/locate/ynicl

Machine-learning classification of 22q11.2 deletion syndrome: A diffusion tensor imaging study

Daniel S. Tylee[a,b], Zora Kikinis[c], Thomas P. Quinn[d], Kevin M. Antshel[e], Wanda Fremont[b], Muhammad A. Tahir[b], Anni Zhu[c], Xue Gong[c], Stephen J. Glatt[a,b], Ioana L. Coman[b], Martha E. Shenton[c,f,g], Wendy R. Kates[b,*,1], Nikos Makris[f,h,1]

[a] Department of Neuroscience and Physiology, SUNY Upstate Medical University, Syracuse, NY, USA
[b] Department of Psychiatry and Behavioral Sciences; SUNY Upstate Medical University, Syracuse, NY, USA
[c] Department of Psychiatry, Brigham and Women's Hospital, Harvard Medical School, Boston, MA, USA
[d] Bioinformatics Core Research Group, Deakin University, Geelong, Victoria, Australia
[e] Syracuse University, Syracuse, NY, USA
[f] Department of Radiology, Brigham and Women's Hospital, Harvard Medical School, Boston, MA, USA
[g] VA Boston Healthcare System, Harvard Medical School, Brockton, MA, USA
[h] Department of Psychiatry, Massachusetts General Hospital, Harvard Medical School, Boston, MA, USA

ARTICLE INFO

Keywords:
22q11.2 deletion syndrome
Velocardiofacial syndrome
Diffusion tensor imaging
White matter query language
Machine-learning
Support vector machine
Inferior longitudinal fasciculus
Middle longitudinal fascicle
Extreme capsule
Callosal asymmetry

ABSTRACT

Chromosome 22q11.2 deletion syndrome (22q11.2DS) is a genetic neurodevelopmental syndrome that has been studied intensively in order to understand relationships between the genetic microdeletion, brain development, cognitive function, and the emergence of psychiatric symptoms. White matter microstructural abnormalities identified using diffusion tensor imaging methods have been reported to affect a variety of neuroanatomical tracts in 22q11.2DS. In the present study, we sought to combine two discovery-based approaches: (1) white matter query language was used to parcellate the brain's white matter into tracts connecting pairs of 34, bilateral cortical regions and (2) the diffusion imaging characteristics of the resulting tracts were analyzed using a machine-learning method called support vector machine in order to optimize the selection of a set of imaging features that maximally discriminated 22q11.2DS and comparison subjects. With this unique approach, we both confirmed previously-recognized 22q11.2DS-related abnormalities in the inferior longitudinal fasciculus (ILF), and identified, for the first time, 22q11.2DS-related anomalies in the middle longitudinal fascicle and the extreme capsule, which may have been overlooked in previous, hypothesis-guided studies. We further observed that, in participants with 22q11.2DS, ILF metrics were significantly associated with positive prodromal symptoms of psychosis.

1. Introduction

Chromosome 22q11.2 deletion syndrome (22q11.2DS; also known as velo-cardio-facial syndrome or DiGeorge syndrome) is a genetic neurodevelopmental disorder that occurs from an interstitial deletion of 40–50 genes on the long arm of chromosome 22. Individuals with 22q11.2DS often experience cardiac and craniofacial anomalies, as well as learning difficulties, diminished trajectories of intellectual development, and difficulties with executive function, social skills, and emotion regulation (e.g., Antshel et al., 2005; Campbell et al., 2015; Duijff et al., 2012; Simon et al., 2002; Swillen et al., 1997). Additionally, a sizeable minority (20–30%) of individuals with 22q11.2DS go on to develop psychotic disorders, including schizophrenia, in young adulthood (e.g., Bassett et al., 2005; Murphy et al., 1999; Schneider et al., 2014). Given

Abbreviations: (22q11.2DS), 22q11.2 deletion syndrome; (AD), axial diffusivity; (DTI), diffusion tensor imaging; (DWI), diffusion weighted image; (dTP), dorsal temporal pole; (EmC), extreme capsule; (FOV), field of view; (FA), fractional anisotropy; (-fp), fronto-parietal aspect; (GDS), Gordon Diagnostic Systems; (ILF), inferior longitudinal fasciculus; (MdLF), middle longitudinal fascicle; (RD), radial diffusivity; (ROI), region of interest; (SRS), Social Responsiveness Scale; (SIPS), Structured Interview for Prodromal Syndromes; (STG), superior temporal gyrus; (SVM), support vector machine; (-to), temporo-occipital aspect; (-tp), temporo-parietal aspect; (UKF), Unscented Kalman Filter; (WAIS-III), Wechsler Adult Intelligence Scale – 3rd edition; (WMQL), white matter query language

* Corresponding author at: Department of Psychiatry, SUNY Upstate Medical University, 750 E. Adams St., Syracuse, NY 13210, USA.
E-mail addresses: zora@bwh.harvard.edu (Z. Kikinis), kmantshe@syr.edu (K.M. Antshel), fremontw@upstate.edu (W. Fremont), stephen.glatt@psychgenelab.com (S.J. Glatt), comani@upstate.edu (I.L. Coman), shenton@bwh.harvard.edu (M.E. Shenton), katesw@upstate.edu (W.R. Kates), nikos@nmr.mgh.harvard.edu (N. Makris).
[1] The two last authors contributed equally to this study and share senior authorship.

http://dx.doi.org/10.1016/j.nicl.2017.04.029
Received 26 February 2017; Received in revised form 27 March 2017; Accepted 4 April 2017
Available online 11 May 2017

the increased risk for schizophrenia among individuals with 22q11.2DS, researchers have explored the links between this genetic deletion, brain development, and the manifestation of psychotic symptoms.

A growing body of neuroimaging research has helped to characterize gray and white matter abnormalities in individuals with 22q11.2DS, with evidence for both reductions in gray matter and total brain volumes (Campbell et al., 2006; Dufour et al., 2008; Gothelf et al., 2011), as well as reductions in white matter volumes (van Amelsvoort et al., 2001; Baker et al., 2011; Campbell et al., 2006; Kates et al., 2001; Da Silva Alves et al., 2011). A meta-analysis further highlighted volumetric white matter abnormalities in temporal, parietal, and occipital lobes (Tan et al., 2009). More recently, diffusion tensor imaging (DTI) methods have made it possible to evaluate white matter microstructure by measuring the magnitude and direction of water diffusion in three dimensions throughout brain tissues. This approach typically examines 22q11.2DS-related differences using several parameters, including (1) fractional anisotropy (FA), which measures the extent to which diffusion is directionally restricted, and which may be diminished under conditions of insult or damage to white matter; (2) radial diffusivity (RD), which is thought to be associated with the modulation of myelin in white matter; and (3) axial diffusivity (AD), purportedly associated with axonal loss or disorganization (Budde et al., 2009; Song et al., 2005). Briefly, the extant literature suggests that 22q11.2DS is characterized by alterations in several white matter tracts. Although results have not always converged, due in part to the application of different whole brain and tractography methods, variable age groups, and small samples (Scariati et al., 2016), most studies point to structural dysconnectivity of brain networks that have been implicated in visual spatial skills, language functions, and schizophrenia (Váša et al., 2016). Specifically, alterations in FA, RD and AD have been observed in individuals with 22q11.2DS in interhemispheric (i.e., callosal) tracts (Bakker et al., 2016; Jalbrzikowski et al., 2014; Kikinis et al., 2016; Simon et al., 2005; Villalon-Reina et al., 2013), and long range, anterior-posterior tracts such as the superior longitudinal fasciculus (Kikinis et al., 2016; Villalon-Reina et al., 2013), the inferior longitudinal fasciculus (Kikinis et al., 2013; Villalon-Reina et al., 2013), and the inferior frontal-occipital fasciculus (Jalbrzikowski et al., 2014; Kikinis et al., 2013). Alterations have also been noted consistently in intra-frontal, intra-parietal and intra-temporal tracts (Barnea-Goraly et al., 2003, 2005; Ottet et al., 2013; Da Silva Alves et al., 2011; Simon et al., 2008), uncinate fasciculus (Radoeva et al., 2012), cingulum (Jalbrzikowski et al., 2014; Kates et al., 2015; Kikinis et al., 2012; Simon et al., 2005), fornix (Deng et al., 2015; Perlstein et al., 2014), anterior (Perlstein et al., 2014; Sundram et al., 2010) and posterior (Jalbrzikowski et al., 2014) limbs of the internal capsule, and both corona radiata and anterior thalamic radiation (Bakker et al., 2016; Jalbrzikowski et al., 2014; Kikinis et al., 2016; Sundram et al., 2010; Villalon-Reina et al., 2013). This body of literature has been reviewed previously (Dennis and Thompson, 2013; Scariati et al., 2016).

Given such strong evidence of DTI abnormalities in 22q11.2DS generally, the goal of the present study was to employ a discovery-based approach to identify a set of white matter tracts that maximally discriminates 22q11.2DS from control subjects and to potentially shed new light on tracts that were not explicitly examined in previous studies. We applied two separate discovery-based approaches to our data. First, as described in detail below, we utilized a method called white matter query language (Wassermann et al., 2013, 2016) to generate diffusion imaging metrics (i.e., FA, AD, RD, trace, and number of streamlines) for white matter tracts between each of 34 atlas-based (Desikan et al., 2006) regions of interest (ROI's) per brain hemisphere. This permitted us to examine the integrity and discriminative ability of white matter tracts that may not have been previously investigated or reported in individuals with 22q11.2DS. Second, we analyzed our resultant diffusion imaging metrics with a type of machine-learning algorithm called a support vector machine (SVM), which can accommodate multiple diffusion imaging measurements and can model their interactions in high dimensional space in order to optimize the classification of the two groups. The combination of these methods extends previous studies by examining the full scope of white matter tracts that are potentially altered in 22q11.2DS-affected individuals relative to healthy controls. For tracts that were significantly altered in probands, we assessed correlations with clinical measures in order to examine the extent to which those alterations may be driving cognitive and psychiatric impairments in individuals with this syndrome.

There is a considerable body of literature examining the application of machine-learning methods such as SVM with neuroimaging data for the purpose of clinical prediction related to psychiatric, neurological, and neurodevelopmental conditions (for reviews, see Fu and Costafreda, 2013; Orrù et al., 2012). Of note, a relatively smaller group of studies supports the potential utility of using diffusion imaging data for making clinical predictions related to diagnostic status, functional capacity, and future prognosis (e.g., Ciulli et al., 2016; Dyrba et al., 2015; Fang et al., 2012; Haller et al., 2010, 2012; Ingalhalikar et al., 2011; Li et al., 2014; O'Dwyer et al., 2012; Peruzzo et al., 2015; Pettersson-Yeo et al., 2013). To our knowledge, no previous studies have applied machine-learning methods in combination with diffusion imaging data to samples of individuals with 22q11.2DS.

2. Methods

2.1. Participants

The imaging data presented in this study were derived from a subsample of participants enrolled in a longitudinal study of risk factors for psychosis in 22q11.2DS (Kates et al., 2004). Several papers examining white matter microstructure have been published on this cohort based on assessments at the third timepoint of the study, while subjects were between the ages of 15 and 21 (Kates et al., 2015; Kikinis et al., 2016; Perlstein et al., 2014; Radoeva et al., 2012). However, the current study examines white matter microstructure based on participant assessments at the 4th timepoint of the study, when subjects were between the ages of 18 and 24 years. Moreover, whereas previous papers were based on imaging data acquired from a 1.5 Tesla scanner, the current set of analyses are based on data acquired from a 3 Tesla scanner, utilizing state-of-the-art two-tensor tractography to measure white matter microstructure.

The present subsample consists of all participants who returned for the fourth timepoint of the study, including 56 participants with 22q11.2DS, 12 unaffected siblings, and 18 community controls. Participants were recruited from the International Center for Evaluation, Treatment, and Study of Velo-Cardio-Facial Syndrome at SUNY Upstate Medical University, parent support groups, and the surrounding community. Presence of the 22q11.2 deletion was confirmed with fluorescence in situ hybridization (FISH). Informed consent was obtained under protocols approved by the medical center's institutional review board. Since siblings and community controls did not differ significantly in age ($p = 0.12$), gender distribution ($p = 0.91$), or full scale IQ ($p = 0.33$), we combined the sibling and community controls into one control group, consisting of 30 participants, for the remainder of the analyses (Table 1). We also demonstrated that siblings and community controls showed minimal differences in diffusion imaging data that discriminated individuals with and without 22q11.2DS (Supplementary Table 1).

2.2. MRI acquisition/DTI processing

2.2.1. Scan acquisitions

For the fourth study timepoint, images were acquired using a 3T Siemens Magnetom Tim Trio scanner (Siemens Medical Solutions, Erlangen, Germany). The high resolution anatomic scan consisted of an ultrafast gradient echo 3D sequence (MPRAGE) with PAT k-space-based

Table 1
Sample demographic and clinical features.

	22q11.2DS (n = 56)	Combined control (n = 30)	Test statistics
Age	20.9 ± 2.3	21.0 ± 1.5	$t = 0.13$, $p = 0.89$
n female	26	14	$\chi^2 = 0$, $p = 1$
n Caucasian	49	25	$\chi^2 = 0.49$, $p = 0.48$
Full Scale IQ	74.3 ± 11.8	109.5 ± 16.0	$F = 10.6$, $p = 6.2 \times 10^{-14}$
n prodromal/ psychosis symptoms	15	0	–

Values are depicted as mean + s.d. Abbreviations: Individuals affected by 22q11.2 deletion syndrome (22q11.2DS).

algorithm GRAPPA. The parameters included: echo time = 3.31 ms; repetition time = 2530 ms; matrix size = 256 × 256; field of view (FOV) = 256 mm; slice thickness = 1 mm. The DTI sequence consisted of 64 transverse slices with no gaps and 2.0 mm nominal isotropic resolution (TR/TE = 8600/93 ms, FOV = 244 × 244, data matrix = 96 × 96, zero-filled and reconstructed to 256 × 256). Diffusion weighting was applied along 64 directions with a $\boldsymbol{b}$ factor = 700 s/mm^2. One minimally weighted volume (b_0) was acquired within each DTI dataset. The total scan time to acquire the DTI dataset was 4 min and 52 s. A high resolution T2 scan was also obtained to align with the diffusion images.

2.2.2. Diffusion tensor imaging preprocessing

We utilized an in-house script to correct for eddy current distortions and head motion. Using an affine transformation, this script registered each diffusion-weighted volume to the baseline volume using FSL (http://fsl.fmrib.ox.ac.uk) linear registration software "FLIRT".

2.2.3. Whole brain tractography

We applied a two-tensor tractography protocol to determine white matter tracts/bundles (Rathi et al., 2011). Relative to one-tensor methods, two-tensor tractography features better fiber representation in both fiber branching and fiber crossing by computing two tensors for each voxel (Malcolm et al., 2010a). Fiber tracts were generated from diffusion weighted images (DWI) using the Unscented Kalman Filter (UKF) based on a two-tensor tractography algorithm (Malcolm et al., 2010b). Tract seeding was completed in every voxel where the primary single tensor fractional anisotropy (FA) value was larger than 0.18, with each voxel seeded 10 times. Fibers between neighboring voxels were traced following the direction of the primary tensor component. Fibers were terminated when the primary tensor FA value was < 0.15.

2.2.4. FreeSurfer parcellations and registration to DTI space

We used FreeSurfer software (http://surfer.nmr.mgh.harvard.edu) to obtain regions of interest via an automated approach, which segmented T1-weighted MPRAGE images into 34 bilateral, cortical and white matter regions for each participant (Fischl et al., 2004). For each of the participants, the label map with FreeSurfer-generated regions of interest was registered to the DWI space by first diffeomorphically registering a T2 image in the same space as the MPRAGE image to the baseline DWI image of the same participant using the FLIRT algorithm of the FSL software (Smith et al., 2004), and then applying this diffeomorphism to register the FreeSurfer-generated label map to the DWI space for the same participant.

2.2.5. White matter query language

White matter query language (WMQL) was used to extract fiber tracts from the two-tensor whole brain tractography (Wassermann et al., 2013, 2016). WMQL was designed to estimate fiber tracts using neuroanatomical definitions. Fiber tract definitions were based on cortical regions where the fibers begin and end, as well as on white matter regions where the fiber tract is expected to project. These definitions were based on the FreeSurfer-generated parcellations of cortical gray matter and white matter regions (Wassermann et al., 2013). Accordingly, for each participant, we generated diffusion metrics for white matter tracts between all 34, FreeSurfer-generated, left hemisphere, right hemisphere, and cross-hemisphere regions of interest. However, WMQL also allowed us to calculate the number of streamlines for each tract, and only tracts with > 10 streamlines were reported. This yielded metrics on a total of 2037 tracts per participant. The diffusion metrics of FA, axial diffusivity (AD), radial diffusivity (RD), trace and number of streamlines were extracted from the entire fiber tract and mean values were computed.

2.3. Machine-learning classification

We use the term "feature" to describe any diffusion imaging metric that was quantified for every subject and could be supplied to machine-learning algorithms for classification. For the present study, we examined only features that were measured above detection threshold for all subjects (thus reducing the application of our machine-learning algorithms to a total of 573 unique combinations of white matter tracts and tract features). These features included (1) the estimated number of fibers, (2) the mean FA, (3) the mean trace, (4) the mean RD, and (5) the mean AD for each tract. We constructed and independently validated the support vector machine classifiers using a custom-built pipeline based on a publicly available machine learning suite for R (Quinn et al., 2016). Code for this classification pipeline is available upon request to the corresponding author.

Individuals were pseudo-randomly selected for the training sample (n = 58, reflecting 67% of subjects). This sample was exactly balanced for the number of 22q11.2DS-affected individuals and non-affected controls, such that they were not significantly different in age (t-test $p > 0.25$) or sex (chi-squared $p > 0.25$). All feature selection and model fitting was performed within the training sample. The training sample was bootstrapped five times to produce alternate versions of the training data. Within each bootstrap, features were selected using several methods, including t-tests, Kolmogorov–Smirnov tests, recursive feature elimination (Guyon et al., 2002), minimum redundancy maximum relevance (De Jay et al., 2013), and empirical Bayesian feature selection (Ritchie et al., 2015). The resulting features selected by each method were combined with a linear kernel SVM (Meyer et al., 2015) systematically tested over a grid of possible settings for cost penalty. The classification accuracy of each resulting model was evaluated using 5-fold cross-validation within the training set and the best performing model was selected from each of the five bootstrap; these were combined to create a prediction ensemble where the probabilistic decisions from the machines were averaged to make a final decision for each new data point tested.

The counterpart validation sample contained the remaining 33% of subjects (n = 28). This sample was not part of the initial model fitting but was instead used to evaluate the ensemble of best models developed in the training set. We repeated this procedure twenty times, each time assigning different subjects to the training and validation set, in order to obtain a robust estimate of classification accuracy. We then examined which features were most consistently selected within the twenty resulting classification ensembles. We followed up our machine-learning analyses with t-tests comparing the two study groups on those features that were consistently selected within the machine-learning ensembles.

2.4. Visual inspection/quality control

All ROI – to – ROI connections that significantly discriminated individuals with 22q11.2DS from controls were reconstructed using the image processing program, 3D Slicer, and were visually inspected for

the imaging datasets of all study participants by our neuroanatomist (N.M.) and diffusion imaging specialist (Z.K.) These visual inspections served to confirm that the location of these connections corresponded to specific fiber tracts that have been previously described in primate, histological, and diffusion imaging literatures (Catani et al., 2005; Dejerine, 1895; Ludwig and Klingler, 1956; Makris et al., 2016; Makris, 1999; Makris et al., 1997, 1999, 2005, 2009; Makris and Pandya, 2009; Schmahmann et al., 2007; de Schotten et al., 2011).

2.5. Clinical data and correlations with diffusion imaging features

For diffusion imaging features that were consistently selected within machine-learning predictive ensembles, we sought to examine whether those features were correlated with clinical measures obtained at timepoint four. We chose clinical measures reflecting constructs that have been previously associated with the particular white matter tracts selected by machine learning algorithms (as described in Results). Unless otherwise noted, we used Pearson correlations to assess relationships with diffusion measures in the full sample, and we repeated these analyses in control-only and 22q11.2-DS-only subsets. Clinical measures examined for the present set of analyses included attention, which was assessed with a continuous performance test, the Gordon Diagnostic System (GDS); the Omission score from the Vigilance task was used for the present analyses (Gordon, 1983). Additionally, we examined prodromal symptoms of psychosis with several subtotal items from the Structured Interview for Prodromal Syndromes (SIPS; Miller et al., 2003), including Disorganized, Negative, and Positive Subscale scores. The SIPS items are based on count data and tend to contain an abundance of zeros. These relationships were assessed using Poisson regression in the 22q11.2DS-only subset. We examined the total impairment score derived from the Social Responsiveness Scale (SRS; Constantino et al., 2003). Additionally, from the Wechsler Adult Intelligence Scale – 3rd edition (WAIS-III; Wechsler, 1997), we examined composite scores for working memory, perceptual organization, processing speed, and verbal comprehension.

3. Results

The full sample available for classification was composed of fifty-six individuals with 22q11.2DS and 30 unaffected control subjects. Classification accuracy is shown in Table 2. Within the training set, accuracy was high (> 90%), but was somewhat more modest in the validation set (mean accuracy = 0.848 + 0.052%). We identified ten diffusion features (i.e., FA, AD, RD, Trace), reflecting properties of 8 distinct pairs of ROIs, that were selected in ≥ 50% of the machines that discriminated between study groups (Table 3). Across these 10 discriminative features, the indices of mean trace, AD, and RD were generally diminished in the 22q11.2DS-affected individuals, while FA was increased. These differences were robust following Bonferroni-correction for multiple testing (Table 3). Below, we describe the tracts to which these features corresponded, and the clinical measures with which they were associated (also see Table 3).

Table 2
Classification results.

Classification task	Support vector machine
Contrast 1: all control vs. all individuals with 22q11.2DS	Training CV accuracy = 0.911 + 0.029 Validation set accuracy = 0.848 + 0.052 Validation set AUC ROC = 0.890 + 0.041 Validation set sensitivity = 0.848 + 0.053 Validation set specificity = 0.820 + 0.077

All values are depicted as mean + s.d. generated across the 20 pseudorandom re-samplings of training and withheld validation sets. Abbreviations: 22q11.2 deletion syndrome (22q11.2DS), area under the curve (AUC), cross-validation (CV), receiver operating characteristic (ROC).

Features of the inferior longitudinal fasciculus (ILF; temporo-parietal aspect, bilaterally) discriminated individuals with 22q11.2DS from controls, showing evidence for increased FA and diminished RD and mean trace in individuals with 22q11.2DS (Table 3, Fig. 1). In addition, the left-side temporo-occipital aspect of the ILF showed diminished AD in the 22q11.2DS group. Notably, these tracts also showed statistically significant relationships with SIPS scales reflecting disorganization, negative, and positive symptoms. These relationships were especially robust to multiple correction for the right-sided temporo-parietal aspect and the left-sided temporo-occipital aspect of the ILF (Fig. 1E).

We further observed that features of the middle longitudinal fascicle (MdLF; left-side; Fig. 2) and the extreme capsule (EmC; left-side, fronto-parietal and temporo-parietal aspects; Fig. 3) discriminated individuals with 22q11.2DS from controls (Table 3). Both tracts showed diminished mean trace in the 22q11.2DS group. Moreover, the MdLF showed nominally significant correlations with errors of omission in the GDS vigilance task. In addition, two of the unique ROI-to-ROI connections that discriminated study groups in > 50% of the ensembles reflected tracts that passed contralaterally and showed reduced mean trace and increased FA in 22q11.2DS. Since our data suggested, and visual inspection (by N.M. and Z.K.) confirmed they did not connect left-hemisphere gyri to their right hemisphere counterparts as we would expect, we refer to these tracts as callosal asymmetries (Fig. 4).

Finally, nearly all of the discriminative features for the tracts identified above showed significant correlations with WAIS-III composite scores for working memory, perceptual organization, processing speed, and verbal comprehension, as well as the total impairment score of the SRS; many of these relationships survived correction for multiple testing (Table 3).

4. Discussion

This is the first study, to our knowledge, to use machine learning algorithms to examine a comprehensive set of diffusion imaging features for a sample of individuals with 22q11.2DS. The three tracts that most robustly discriminated individuals with 22q11.2DS from comparison subjects were the inferior longitudinal fasciculus, the middle longitudinal fascicle and the extreme capsule. We further observed that the ILF was robustly, and uniquely, associated with prodromal symptoms of psychosis in our 22q11.2DS sample. Although dysconnectivity of the ILF has been reported previously in 22q11.2DS, our study is the first to observe microstructural alterations in the MdLF and EmC in individuals with this genetic syndrome.

Our unique application of two tensor tractography, along with our discovery-based method by which we measured diffusion imaging parameters along connections between the 34, bilateral regions of interest included in Freesurfer's Desikan atlas, enabled us to visualize white matter tracts to which previous examinations of microstructural alterations in individuals with 22q11.2DS may not have had access. Moreover, our use of support vector machine algorithms permitted us to test multiple iterations of feature ensembles to identify the features that most robustly discriminated young adults with 22q11.2DS from controls. Taken together, our image processing and analysis methods enabled us to demonstrate the classification accuracy of three association fiber tracts that differentiated our two samples.

The ILF, a long association fiber tract (Catani et al., 2003; Dejerine, 1895; Ludwig and Klingler, 1956; Makris et al., 1997, 1999), which extends from the parietal and occipital lobe to lateral and ventral regions of the temporal lobe (Makris et al., 1999; Schmahmann et al., 2007), has been implicated in several studies of white matter microstructure in individuals with 22q11.2DS. Specifically, our finding that AD and RD was decreased in individuals with 22q11.2DS is consistent with previous reports (Jalbrzikowski et al., 2014; Kikinis et al., 2012; Simon et al., 2008). In contrast, the increase in FA that we observed is at odds with several reports of decrease in FA in 22q11.2DS (Kikinis et al., 2012, 2013; Sundram et al., 2010; Villalon-Reina et al., 2013).

Table 3
22q11.2DS-related diffusion imaging features.

ROI–to–ROI connection	dMRI measure	Test statistic	Group means (control, 22q11.2Ds)	Fiber bundles	Significant clinical correlations (all subjects)						
					GDS vigilance omissions		SRS total impairment score		WAIS-III working memory		WAIS-III perceptual organization
					r	*p*-Value	*r*	*p*-Value	*r*	*p*-Value	*r*
(L) Inferior parietal cortex to (L) middle temporal cortex	FA mean	$t = -5.04$ $p = 5.7 \times 10^{-6*}$	611.54 ± 29.11 643.42 ± 25.63	(L) ILF-tp	–	–	0.34	1.4×10^{-3}	-0.37	$4.4 \times 10^{-4*}$	-0.43
	Mean trace	$t = 6.96$ $p = 5.2 \times 10^{-9*}$	2.35 ± 0.08 2.23 ± 0.07	(L) ILF-tp	–	–	-0.33	2.2×10^{-3}	0.35	9.7×10^{-4}	0.46
	RD mean	$t = 6.30$ $p = 6.4 \times 10^{-8*}$	460.59 ± 34.13 414.26 ± 29.24	(L) ILF-tp	–	–	-0.35	1.1×10^{-3}	0.38	$2.6 \times 10^{-4*}$	0.47
(L) Inferior parietal cortex to (L) superior temporal cortex	Mean trace	$t = 7.17$ $p = 1.5 \times 10^{-9*}$	2.39 ± 0.08 2.26 ± 0.08	(L) MdLF, MdLF/EmC-tp	0.23	3.3×10^{-2}	-0.40	$1.3 \times 10^{-4*}$	0.32	2.6×10^{-3}	0.48
(L) Inferior parietal cortex to (L) insular cortex	Mean trace	$t = 7.19$ $p = 3.0 \times 10^{-9*}$	2.4 ± 0.08 2.28 ± 0.06	(L) EmC-fp/tp	–	–	-0.43	$4.9 \times 10^{-5*}$	0.36	7.2×10^{-4}	0.53
(L) Inferior temporal cortex to (L) lateral occipital cortex	AD mean	$t = 5.02$ $p = 5.1 \times 10^{-6*}$	1486.01 ± 50.25 1429.2 ± 49.6	(L) ILF-to	–	–	-0.38	$3.2 \times 10^{-4*}$	0.30	5.2×10^{-3}	0.37
(L) Paracentral cortex to (R) precentral cortex	Mean trace	$t = 7.09$ $p = 2.8 \times 10^{-9*}$	2.38 + 0.09 2.24 + 0.08	Callosal asymmetry	–	–	-0.43	$3.4 \times 10^{-5*}$	0.47	$4.4 \times 10^{-6*}$	0.55
(L) Precentral cortex to (R) superior frontal cortex	FA mean	$t = -4.78$ $p = 1.3 \times 10^{-5*}$	683.04 + 23.39 707.77 + 21.77	SLF (frontal aspect) asymmetry	-0.24	2.4×10^{-2}	0.31	4.5×10^{-3}	-0.38	$3.5 \times 10^{-4*}$	-0.41
(R) Inferior parietal cortex to (R) middle temporal cortex	FA mean	$t = -6.06$ $p = 7.7 \times 10^{-8*}$	630.08 ± 20.19 658.85 ± 22.38	(R) ILF-tp	-0.24	2.5×10^{-2}	0.47	$6.0 \times 10^{-6*}$	-0.43	$3.3 \times 10^{-5*}$	-0.52
(R) Precuneus to (R) insular cortex	FA mean	$t = -5.29$ $p = 1.1 \times \times 10^{-6*}$	606.92 + 24.18 640.35 + 33.9	EmC	–	–	0.25	2.2×10^{-2}	-0.33	2.1×10^{-2}	-0.37

ROI–to–ROI connection	Significant clinical correlations (all subjects)					Significant clinical correlations (22q11.2DS subjects)					
	WAIS-III perceptual organization	WAIS-III processing speed		WAIS-III verbal comprehension		SIPS subtotal disorganized symptoms		SIPS subtotal negative symptoms		SIPS subtotal positive symptoms	
	p-Value	*r*	*p*-Value	*r*	*p*-Value	ß	*p*-Value	ß	*p*-Value	ß	*p*-Value
(L) Inferior parietal cortex to (L) middle temporal cortex	$3.7 \times 10^{-5*}$	-0.30	4.3×10^{-3}	-0.42	$5.1 \times 10^{-5*}$	–	–	0.00	3.4×10^{-2}	–	–
	$7.2 \times 10^{-6*}$	0.29	7.2×10^{-3}	0.38	$3.0 \times 10^{-4*}$	2.53	6.3×10^{-3}	3.10	1.3×10^{-3}	–	–
	$5.0 \times 10^{-5*}$	0.31	3.5×10^{-3}	0.43	$4.3 \times 10^{-5*}$	–	–	–	–	0.00	2.3×10^{-2}
(L) Inferior parietal cortex to (L) superior temporal cortex	$3.7 \times 10^{-6*}$	0.33	1.9×10^{-3}	0.38	$3.3 \times 10^{-4*}$	–	–	-2.00	1.6×10^{-3}	-2.24	1.2×10^{-2}
(L) Inferior parietal cortex to (L) insular cortex	$1.4 \times 10^{-7*}$	0.40	$1.2 \times 10^{-4*}$	0.48	$3.4 \times 10^{-5*}$	–	–	-2.79	5.7×10^{-4}	-2.74	1.7×10^{-3}
(L) Inferior temporal cortex to (L) lateral occipital cortex	$4.0 \times 10^{-4*}$	0.32	2.6×10^{-3}	0.29	7.0×10^{-3}	-0.01	0.0018	-0.01	$2.6 \times 10^{-5*}$	-0.01	$3.1 \times 10^{-11*}$
(L) Paracentral cortex to (R) precentral cortex	$4.0 \times 10^{-4*}$	0.43	$4.4 \times 10^{-5*}$	0.47	$5.6 \times 10^{-6*}$	-1.97	0.0022	–	–	–	–
(L) Precentral cortex to (R) superior frontal cortex	$1.1 \times 10^{-4*}$	-0.27	1.8×10^{-2}	-0.39	$1.9 \times 10^{-5*}$	–	–	–	–	–	–
(R) Inferior parietal cortex to (R) middle temporal cortex	$2.9 \times 10^{-7*}$	-0.41	$7.8 \times 10^{-5*}$	-0.39	2.4×10^{-4}	0.01	2.9×10^{-3}	0.01	$2.9 \times 10^{-8*}$	0.02	$1.0 \times 10^{-7*}$
(R) Precuneus to (R) insular cortex	$4.7 \times 10^{-4*}$	-0.32	2.9×10^{-2}	-0.32	2.9×10^{-3}	–	–	–	–	–	–

t-Tests were to compare 22q11.2DS-affected and control subjects for key DTI tract measurements selected in the machine learning study. *p*-Values that survived Bonferroni correction for the total number of features (i.e., 10) are denoted with *. †For clinical correlations, clinical items derived from the Structured Interview for prodromal symptoms were predicted using zero-inflated Poisson regression, with corresponding β coefficient. All other clinical items were analyzed using Pearson correlations. Correlations that survived Bonferroni correction for the total number of correlations (i.e., 10 tracts and 9 clinical items for a total of 90) are denoted with *. Abbreviations: 22q11.2 deletion syndrome-affected individuals (22q11.2DS); axial diffusivity (AD), fractional anisotropy (FA), radial diffusivity, (RD); extreme capsule (EmC), inferior longitudinal fasciculus (ILF), middle longitudinal fasciculus (MdLF), superior longitudinal fasciculus (SLF); fronto-parietal (-fp) temporal-occipital (-to), temporal-parietal (-tp); Global Deficit Score (GDS), Social Responsiveness Scale (SRS), structured interview for prodromal symptoms (SIPS), Wechsler Adult Intelligence Scale (WAIS).

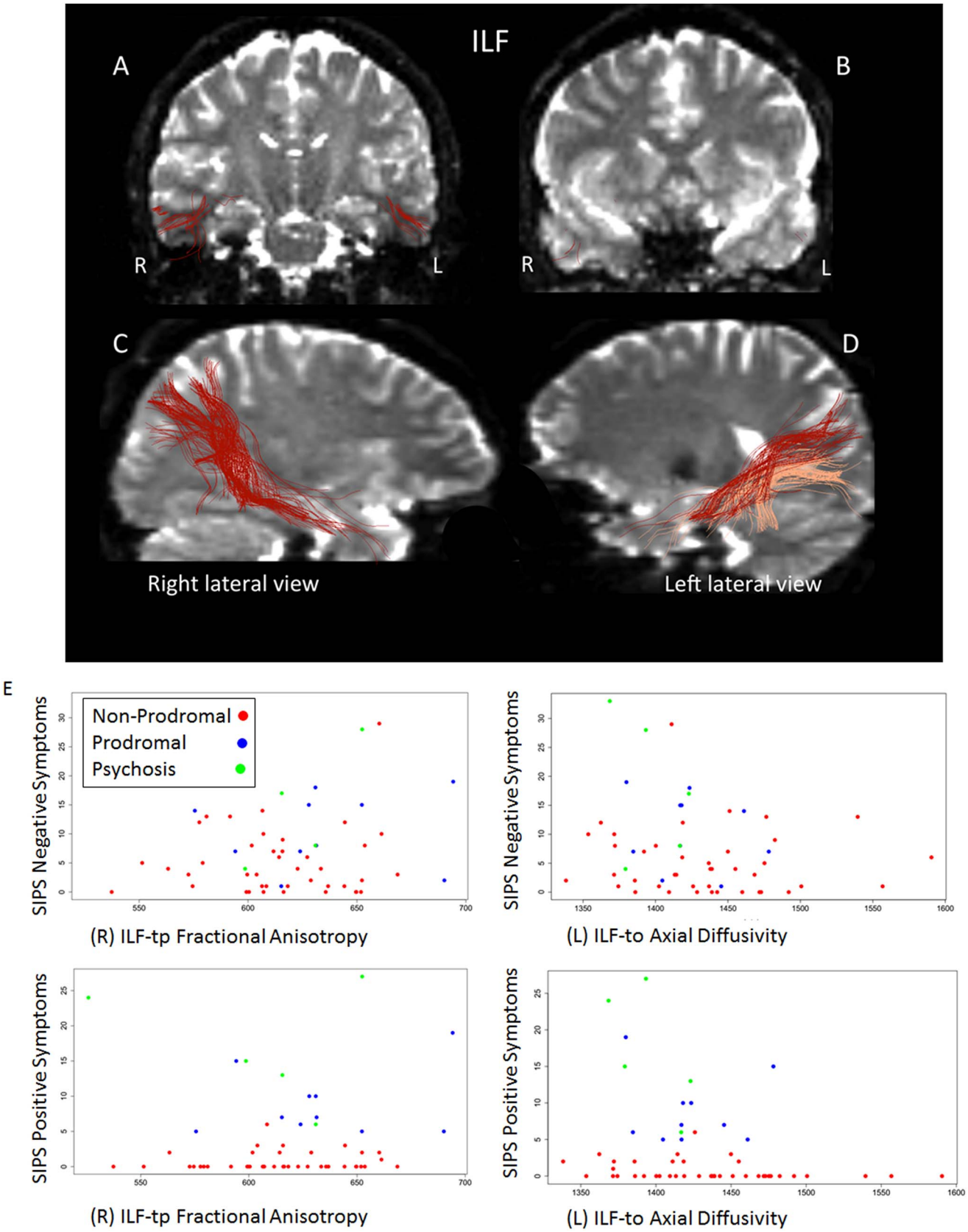

Fig. 1. The right (R) and left (L) inferior longitudinal fasciculi (ILF) are shown in coronal (panels A and B) and lateral views (panels C and D). In panel A, the location of the ILF within the stem of the temporal lobe white matter as well as the middle temporal and inferior temporal gyri white matter is shown. In panel B, the location of ILF fibers in the lateral and ventral parts of the temporal pole is depicted. In panel C, the temporo-parietal connections of ILF are shown in red. Likewise, the temporo-parietal connections of ILF are shown in red in panel D, whereas the temporo-occipital connections of ILF are shown in salmon color. The scatterplots (Panel E) portrays ILF diffusion imaging properties that were frequently selected by learning machines and significantly different between 22q11.2DS and comparison subjects, and depicts significant relationships (see Table 3) with the severity of symptoms measured by Structured Interview for Prodromal Syndromes (SIPS) scales.

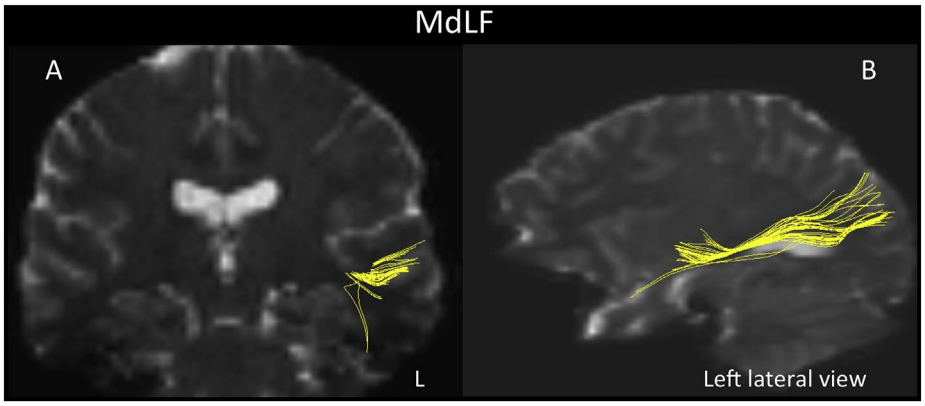

Fig. 2. The left middle longitudinal fascicle (MdLF) is shown in coronal (panel A) and lateral views (panel B) in yellow. In panel A, the location of MdLF in the core white matter of the superior temporal gyrus is shown, whereas its longitudinal trajectory between the superior temporal gyrus (including the dorsal part of the temporal pole) with the inferior parietal lobule (angular gyrus) is indicated. L = left.

One potential explanation for this inconsistency is that our atlas based approach to the generation of white matter tract parameters permitted us to differentiate between the temporo-parietal and the temporo-occipital aspects of the ILF, for which increases in FA were limited to its temporo-parietal aspect. Previous investigations of the ILF may not have been as fine-grained.

The ILF is a major pathway connecting neuroanatomic regions that comprise the ventral visual stream (Saur et al., 2008; Schmahmann and Pandya, 2006), which primarily subserves the functions of object recognition and facial emotion perception (Schmahmann and Pandya, 2006), which have been reported to be impaired in individuals with 22q11.2DS (McCabe et al., 2016). Importantly, alterations of the ILF have also been associated with the presence of positive symptoms of psychosis in people with non-syndromic, early course (Ashtari et al., 2007; Seitz et al., 2016) and chronic schizophrenia (Phillips et al., 2009), as well as individuals with 22q11.2DS (Da Silva Alves et al., 2011). This is consistent with our finding of robust and tract - specific associations between alterations in FA (temporo-parietal component)

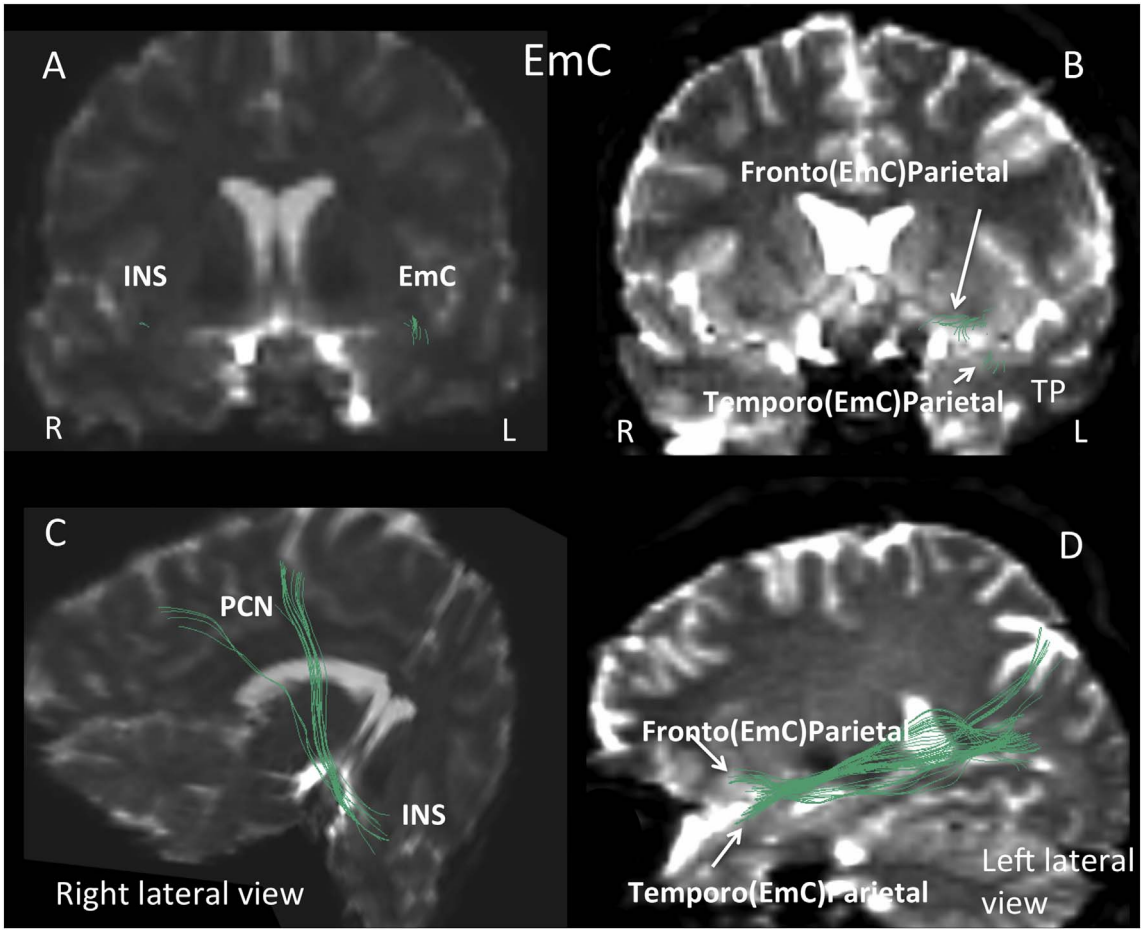

Fig. 3. The extreme capsule (EmC) is shown in coronal (panels A and B), oblique (panel C) and lateral (panel D) views in green. EmC connections between the insula and the precuneus are present in the right (R) hemisphere (panel A and C). The fronto-parietal and temporo-parietal connections of the EmC are depicted on the left (L) hemisphere and are labeled Fronto (EmC)Parietal and Temporo(EmC)Parietal respectively (panel B and D). The latter are shown in panel B connecting separately with the frontal and temporo-polar regions and in panel D they bifurcate at the fronto-temporal junction to follow separate trajectories toward frontal and temporo-polar regions. The INS(EmC)PCN connection is shown in panel C using an oblique view and a combination of a coronal and sagittal sections as background, thus allowing the visualization of the precuneus (PCN) in the sagittal section and the insula (INS) in the coronal slice. R = right; L = left; TP = temporal pole.

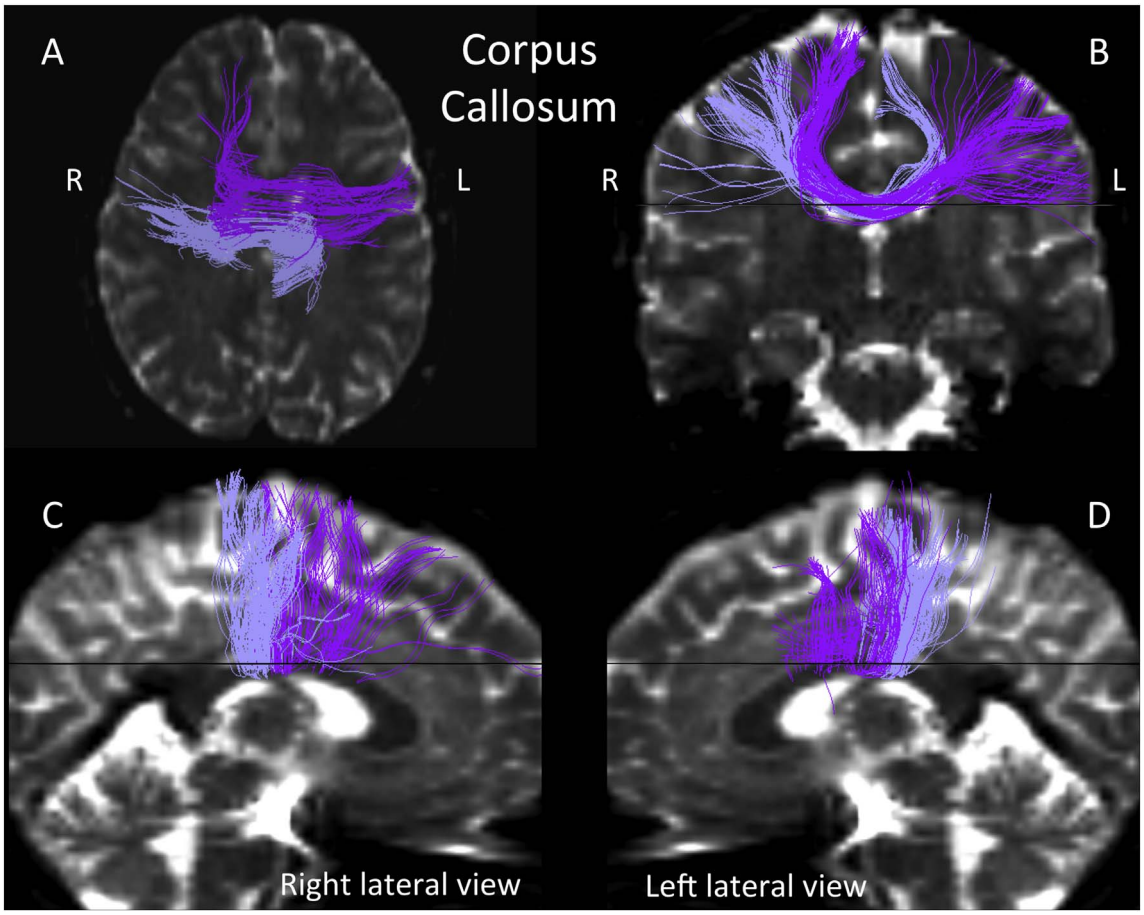

Fig. 4. Asymmetric callosal connections are shown in light blue between the left paracentral lobule and the right precentral gyrus, whereas asymmetric connections between the left precentral gyrus and the right superior frontal gyrus are presented in purple. These fiber connections are viewed from four different perspectives to allow clear inspection. Panel A represents a superior view using an axial plane as background; panel B is a frontal view; panels C and D are lateral views. The black horizontal line in the latter panels represents the level of the axial section of panel A. R = right; L = left.

and AD (temporo-occipital component) of the ILF and both positive and negative symptoms of psychosis in individuals with 22q11.2DS. Our results support the notion that disruption of the ILF, which connects several neuroanatomic regions that have been associated with the pathophysiology of schizophrenia (Catani et al., 2003; Phillips et al., 2009), may underlie not only cognitive deficits but also propensity toward psychosis in individuals with this syndrome.

The MdLF is a long association cortico-cortical fiber tract, which connects the superior temporal gyrus (STG) and dorsal temporal pole (dTP) with the inferior parietal lobule (Makris et al., 2009) that has been discovered in humans recently (Makris, 1999; Makris et al., 2009). Several studies have confirmed and expanded these original observations in more recent DTI tractographic studies demonstrating that the MdLF is comprised of multiple components that interconnect the STG and dTP not only with the angular gyrus, but also with other associative cortical regions of the parietal and occipital lobes, including the supramarginal gyrus, superior parietal lobule, precuneus, cuneus and lateral occipital region (Makris et al., 2013a, 2013b, 2016; Maldonado et al., 2013; Menjot de Champfleur et al., 2013; Wang et al., 2013). The MdLF is located ventral to the superior longitudinal fascicle II (Makris et al., 2005) and dorsal to the inferior longitudinal fasciculus, a fact in its relative topographic anatomy with respect to SLF and ILF, that contributed to its naming as “middle” in the rhesus monkey (Seltzer and Pandya, 1984) and the human (Makris, 1999; Makris et al., 2009). The delineation of multiple components of the MdLF has led investigators to hypothesize that this tract may support language, visual spatial and attention functions (Makris et al., 2009; Makris and Pandya, 2009). Furthermore, a study by Mesulam and colleagues (Mesulam et al., 2015) showed that the left anterior temporal lobe (including the temporal pole) is involved in word and sentence comprehension. These observations strongly support MdLF's role in the language network, a notion supported also by functional connectivity work by Kellmeyer et al. (2013).

These hypotheses are supported by our observations of significant associations between mean Trace of ROI – to – ROI connections that putatively represent the MdLF and the composite WAIS-III scores of Verbal Comprehension and Perceptual Organization as well as the GDS Omissions score (at trend level). However, it should be noted that the associations we observed between WAIS-III composite scores and mean trace for the MdLF tract were not specific: these associations were also observed for the other tracts that significantly differentiated individuals with 22q11.2DS and controls. It is not surprising that composite scores representing multiple cognitive skills would be subserved by multiple white matter tracts.

Located medially to the MdLF, the EmC long cortico-cortical association fiber tract courses through the extreme capsule region, an anatomical white matter region between the insula and the claustrum, and extends from the inferior frontal cortex to the lateral part of the temporal lobe, especially the superior temporal gyrus, and the inferior parietal lobule (Makris and Pandya, 2009; Schmahmann and Pandya, 2006). In humans, there have been identified three components of the EmC (i.e., frontal, temporal and parietal; Makris and Pandya, 2009). Given the different components of EmC, it seems a useful convention to indicate the peripheral terminations of the specific connection as shown in panels B and D of Fig. 3. We have elaborated upon this convention more generally in other publications of our group (Makris et al., 2013b,

2016). In their structural model of the language circuitry, Makris and Pandya (2009) proposed a novel ventral route consisting of the MdLF and EmC involved in language comprehension (via MdLF) and expression (via the frontotemporal component of EmC), thus complementing the traditional Wernicke-Geschwind model of language processing as elaborated further in Makris and Pandya (2009). In non-human primates, the EmC has been found to connect the inferior frontal gyrus, which is the equivalent to Broca's area in humans in the frontal lobe, with the human equivalent of Wernicke's area in the temporal lobe (Schmahmann and Pandya, 2006). Although this precise a connection can only be inferred on diffusion weighted images, it has led investigators to hypothesize that the EmC supports semantic and syntactic comprehension, thus constituting a core language pathway (Kellmeyer et al., 2013; Kljajevic, 2014; Makris and Pandya, 2009; Saur et al., 2008). Our observations suggested associations between metrics of the EmC and Composite scores of the WAIS-III, but again, these scores represent an amalgam of skills, and their association with the EmC was not specific.

Interestingly, the three tracts that discriminated individuals with 22q11.2DS from controls may represent structural components of the ventral stream for language processing (Hickok and Poeppel, 2004, 2007), which is thought to underlie the interface between language sounds and meaning. It should be noticed, however, that to which extent MdLF is exclusively affiliated with the ventral language stream, remains to be determined with clarity (Pandya et al., 2015). Accordingly, the circuits that comprise the ventral language stream putatively support auditory comprehension and semantic processes. Language impairments have been reported extensively in children with 22q11.2DS (Gerdes et al., 1999; Glaser et al., 2002), and may be associated with alterations of these tracts. Moreover, it has been suggested that auditory hallucinations, a commonly reported symptom in both syndromal and non-syndromal individuals with psychosis, may stem from dysfunction in processing and interpreting speech sounds (Badcock, 2010), which are skills subserved by the ventral language stream. Accordingly, future studies that combine imaging of tracts included in the ventral language stream and specific measures of auditory comprehension and semantic processing in 22q11.2DS are warranted.

As noted above, two virtual connections that significantly discriminated individuals with 22q11.2DS from controls were labeled “callosal asymmetries”. These were contralateral, ROI - to - ROI connections between dissimilar regions (e.g. left precentral cortex to right superior frontal cortex). Although it is known in classical neuroanatomy (see e.g., Dejerine, 1895) that “human interhemispheric connections can be widely heterotopic” (Di Virgilio and Clarke, 1997), this knowledge remains, nevertheless very patchy and unclear, thus not allowing us to confirm whether the callosal virtual fibers observed herein represent real anatomical connections. Consequently, these findings should be viewed with caution, as it is possible that they resulted from image artifact. Accordingly, any interpretation of their significance should await replication in larger samples.

The results of this study should be viewed in the context of its potential limitations. The sample was relatively small for a machine learning analysis. Since our total sample consisted of 86 individuals, dividing the sample into training and validation samples resulted in subsamples of 58 and 28 respectively. This underpowered our machine learning analyses to some extent. However, our follow-up statistical comparisons of the tracts that had significantly discriminated individuals with 22q11.2DS from controls (using Bonferroni-corrected *t*-tests) confirmed our machine learning findings, which mitigates this potential limitation to some extent. A second limitation was that, due to the nature of machine learning analyses, we excluded from analysis all features for ROI – to – ROI connections that were not detected in our whole sample. Accordingly, our final group of features was limited to those for which there was no missing data. Consequently, this may have excluded observations of other potentially significant connections that may have discriminated our study groups. In fact, our preliminary analysis included features that were below detection threshold in some subjects (coded as zero) and this resulted in higher classification accuracy (data not shown).

Despite these limitations, our study not only confirmed that alterations of the ILF in 22q11.2DS may increase susceptibility to psychosis, but also demonstrated alterations in two additional fiber tracts, the MdLF and the EmC, that have not been observed in prior studies of individuals with this genetic syndrome. Moreover, to the extent that these three white matter tracts are critical components of the ventral language stream, our observations emphasize the potential importance of early, cognitive interventions focused on auditory comprehension, semantic processing, and other functions subserved by these tracts. Accordingly, our implementation of two-tensor tractography along with our discovery-based approaches to both image processing and analysis led to findings that can pave the way for future hypothesis – based studies that investigate these language-based tracts more extensively, and lay the groundwork for clinically-relevant cognitive remediation interventions focused on skills subserved by the ventral language stream.

5. Conclusions

The application of discovery-based approaches like white matter query language and machine-learning analysis have the potential to identify the full range of diffusion imaging features that maximally discriminate 22q11.2DS. Using this approach, we confirmed previously-recognized 22q11.2DS-related abnormalities in the inferior longitudinal fasciculus (ILF), and identified for the first time, 22q11.2DS-related anomalies in the middle longitudinal fascicle and the extreme capsule. We further observed that, among participants with 22q11.2DS, ILF metrics were significantly associated with positive prodromal symptoms of psychosis.

Supplementary data to this article can be found online at http://dx.doi.org/10.1016/j.nicl.2017.04.029.

Acknowledgements

The authors declare no conflicts of interest in relation to the present study. We gratefully acknowledge the individuals and families who volunteered to participate in the study. This work was supported by funding from the National Institutes of Health grants MH064824 to WRK, AG042512 and AT008865 to NM, and MH106793 to ZK; and a VA Merit Award to MES.

References

van Amelsvoort, T., Daly, E., Robertson, D., Suckling, J., Ng, V., Critchley, H., et al., 2001. Structural brain abnormalities associated with deletion at chromosome 22q11: quantitative neuroimaging study of adults with velo-cardio-facial syndrome. Br. J. Psychiatry 178, 412–419.

Antshel, K.M., Conchelos, J., Lanzetta, G., Fremont, W., Kates, W.R., 2005. Behavior and corpus callosum morphology relationships in velocardiofacial syndrome (22q11.2 deletion syndrome). Psychiatry Res. Neuroimaging 138, 235–245.

Ashtari, M., Cottone, J., Ardekani, B.A., Cervellione, K., Szeszko, P.R., Wu, J., et al., 2007. Disruption of white matter integrity in the inferior longitudinal fasciculus in adolescents with schizophrenia as revealed by fiber tractography. Arch. Gen. Psychiatry 64, 1270–1280.

Badcock, J.C., 2010. The cognitive neuropsychology of auditory hallucinations: a parallel auditory pathways framework. Schizophr. Bull. 36, 576–584.

Baker, K., Chaddock, C.A., Baldeweg, T., Skuse, D., 2011. Neuroanatomy in adolescents and young adults with 22q11 deletion syndrome: comparison to an IQ-matched group. NeuroImage 55, 491–499.

Bakker, G., Caan, M.W.A., Schluter, R.S., Bloemen, O.J.N., da Silva-Alves, F., de Koning, M.B., et al., 2016. Distinct white-matter aberrations in 22q11.2 deletion syndrome and patients at ultra-high risk for psychosis. Psychol. Med. 46, 2299–2311.

Barnea-Goraly, N., Eliez, S., Menon, V., Bammer, R., Reiss, A.L., 2005. Arithmetic ability and parietal alterations: a diffusion tensor imaging study in velocardiofacial syndrome. Cogn. Brain Res. 25, 735–740.

Barnea-Goraly, N., Menon, V., Krasnow, B., Ko, A., Reiss, A., Eliez, S., 2003. Investigation of white matter structure in velocardiofacial syndrome: a diffusion tensor imaging study. Am. J. Psychiatry 160, 1863–1869.

Bassett, A.S., Chow, E.W.C., Husted, J., Weksberg, R., Caluseriu, O., Webb, G.D., et al., 2005. Clinical features of 78 adults with 22q11 deletion syndrome. Am. J. Med.

Genet. 138 (A), 307–313.
Budde, M.D., Xie, M., Cross, A.H., Song, S.-K., 2009. Axial diffusivity is the primary correlate of axonal injury in the experimental autoimmune encephalomyelitis spinal cord: a quantitative pixelwise analysis. J. Neurosci. 29, 2805–2813.
Campbell, L.E., Daly, E., Toal, F., Stevens, A., Azuma, R., Catani, M., et al., 2006. Brain and behaviour in children with 22q11.2 deletion syndrome: a volumetric and voxel-based morphometry MRI study. Brain 129, 1218–1228.
Campbell, L.E., McCabe, K.L., Melville, J.L., Strutt, P.A., Schall, U., 2015. Social cognition dysfunction in adolescents with 22q11.2 deletion syndrome (velo-cardio-facial syndrome): relationship with executive functioning and social competence/functioning. J. Intellect. Disabil. Res. 59, 845–859.
Catani, M., Jones, D.K., Donato, R., Ffytche, D.H., 2003. Occipito-temporal connections in the human brain. Brain 126, 2093–2107.
Catani, M., Jones, D.K., Ffytche, D.H., 2005. Perisylvian language networks of the human brain. Ann. Neurol. 57, 8–16.
Ciulli, S., Citi, L., Salvadori, E., Valenti, R., Poggesi, A., Inzitari, D., et al., 2016. Prediction of Impaired Performance in Trail Making Test in MCI Patients With Small Vessel Disease Using DTI Data. 20. pp. 1026–1033.
Constantino, J.N., Davis, S.A., Todd, R.D., Schindler, M.K., Gross, M.M., Brophy, S.L., et al., 2003. Validation of a brief quantitative measure of autistic traits: comparison of the social responsiveness scale with the Autism Diagnostic Interview-revised. J. Autism Dev. Disord. 33, 427–433.
Dejerine, J.J., 1895. Anatomie des centres nerveux. Rueff et. Cie, Paris, France.
Deng, Y., Goodrich-Hunsaker, N.J., Cabaral, M., Amaral, D.G., Buonocore, M.H., Harvey, D., et al., 2015. Disrupted fornix integrity in children with chromosome 22q11.2 deletion syndrome. Psychiatry Res. 232, 106–114.
Dennis, E.L., Thompson, P.M., 2013. Typical and atypical brain development: a review of neuroimaging studies. Dialogues Clin. Neurosci. 15, 359–384.
Dufour, F., Schaer, M., Debbané, M., Farhoumand, R., Glaser, B., Eliez, S., 2008. Cingulate gyral reductions are related to low executive functioning and psychotic symptoms in 22q11.2 deletion syndrome. Neuropsychologia 46, 2986–2992.
Duijff, S.N., Klaassen, P.W.J., de Veye, H.F.N.S., Beemer, F.A., Sinnema, G., Vorstman, J.A.S., 2012. Cognitive development in children with 22q11.2 deletion syndrome. Br. J. Psychiatry 200, 462–468.
Dyrba, M., Barkhof, F., Fellgiebel, A., Filippi, M., Hausner, L., Hauenstein, K., et al., 2015. Predicting Prodromal Alzheimer's Disease in Subjects with Mild Cognitive Impairment Using Machine Learning Classification of Multimodal Multicenter Diffusion-tensor and Magnetic Resonance Imaging Data. 25. pp. 738–747.
Fang, P., Zeng, L.L., Shen, H., Wang, L., Li, B., Liu, L., et al., 2012. Increased Cortical-Limbic Anatomical Network Connectivity in Major Depression Revealed by Diffusion Tensor Imaging. pp. 7.
Fischl, B., van der Kouwe, A., Destrieux, C., Halgren, E., Segonne, F., Salat, D.H., Busa, E., Seidman, L., Goldstein, J., Kennedy, D., Caviness, V., Makris, N., Rosen, B., Dale, A.M., 2004. Automatically parcellating the human cerebral cortex. Cereb. Cortex 14, 11–22.
Fu, C.H.Y., Costafreda, S.G., 2013. Neuroimaging-based Biomarkers in Psychiatry: Clinical Opportunities of a Paradigm Shift. 58. pp. 499–508.
Gerdes, M., Solot, C., Wang, P.P., Moss, E., LaRossa, D., Randall, P., et al., 1999. Cognitive and behavior profile of preschool children with chromosome 22q11.2 deletion. Am. J. Med. Genet. 85, 127–133.
Glaser, B., Mumme, D.L., Blasey, C., Morris, M.A., Dahoun, S.P., Antonarakis, S.E., et al., 2002. Language skills in children with velocardiofacial syndrome (deletion 22q11.2). J. Pediatr. 140, 753–758.
Gordon, M., 1983. The Gordon Diagnostic System.
Gothelf, D., Hoeft, F., Ueno, T., Sugiura, L., Lee, A.D., Thompson, P., et al., 2011. Developmental changes in multivariate neuroanatomical patterns that predict risk for psychosis in 22q11.2 deletion syndrome. J. Psychiatr. Res. 45, 322–331.
Guyon, I., Weston, J., Barnhill, S., Vapnik, V., 2002. Gene selection for cancer classification using support vector machines. Mach. Learn. 46, 389–422.
Haller, S., Badoud, S., Nguyen, D., Garibotto, V., Lovblad, K.O., Burkhard, P.R., 2012. Individual Detection of Patients with Parkinson Disease Using Support Vector Machine Analysis of Diffusion Tensor Imaging Data: Initial Results. 33. pp. 2123–2128.
Haller, S., Nguyen, D., Rodriguez, C., Emch, J., Gold, G., Bartsch, A., et al., 2010. Individual Prediction of Cognitive decline in Mild Cognitive Impairment Using Support Vector Machine-based Analysis Of Diffusion Tensor Imaging Data. 22. pp. 315–327.
Hickok, G., Poeppel, D., 2004. Dorsal and ventral streams: a framework for understanding aspects of the functional anatomy of language. Cognition 92, 67–99.
Hickok, G., Poeppel, D., 2007. The cortical organization of speech processing. Nat. Rev. Neurosci. 8, 393–402.
Ingalhalikar, M., Parker, D., Bloy, L., Roberts, T.P.L., Verma, R., 2011. Diffusion Based Abnormality Markers of Pathology: Toward Learned Diagnostic Prediction of ASD. 57. pp. 918–927.
Jalbrzikowski, M., Villalon-Reina, J.E., Karlsgodt, K.H., Senturk, D., Chow, C., Thompson, P.M., et al., 2014. Altered white matter microstructure is associated with social cognition and psychotic symptoms in 22q11.2 microdeletion syndrome. Front. Behav. Neurosci. 8, 393.
Desikan, R.S., Segonne, F., Fischl, B., Quinn, B.T., Dickerson, B.C., Blacker, D., Buckner, R.L., Dale, A.M., Maguire, R.P., Hyman, B.T., Albert, M.S., Killiany, R.J., 2006. An automated labeling system for subdividing the human cerebral cortex on MRI scans into gyral based regions of interest. NeuroImage 31, 968–980.
De Jay, N., Papillon-Cavanagh, S., Olsen, C., El-Hachem, N., Bontempi, G., Haibe-Kains, B., 2013. mRMRe: an R package for parallelized mRMR ensemble feature selection. Bioinformatics 29, 2365–2368.
Kates, W.R., Burnette, C.P., Bessette, B.A., Folley, B.S., Strunge, L., Jabs, E.W., et al., 2004. Frontal and caudate alterations in velocardiofacial syndrome (deletion at chromosome 22q11.2). J. Child Neurol. 19, 337–342.
Kates, W.R., Burnette, C.P., Jabs, E.W., Rutberg, J., Murphy, A.M., Grados, M., et al., 2001. Regional cortical white matter reductions in velocardiofacial syndrome: a volumetric MRI analysis. Biol. Psychiatry 49, 677–684.
Kates, W.R., Olszewski, A.K., Gnirke, M.H., Kikinis, Z., Nelson, J., Antshel, K.M., et al., 2015. White matter microstructural abnormalities of the cingulum bundle in youths with 22q11.2 deletion syndrome: associations with medication, neuropsychological function, and prodromal symptoms of psychosis. Schizophr. Res. 161, 76–84.
Kellmeyer, P., Ziegler, W., Peschke, C., Juliane, E., Schnell, S., Baumgaertner, A., et al., 2013. Fronto-parietal dorsal and ventral pathways in the context of different linguistic manipulations. Brain Lang. 127, 241–250.
Kikinis, Z., Asami, T., Bouix, S., Finn, C.T., Ballinger, T., Tworog-Dube, E., et al., 2012. Reduced fractional anisotropy and axial diffusivity in white matter in 22q11.2 deletion syndrome: a pilot study. Schizophr. Res. 141, 35–39.
Kikinis, Z., Cho, K.I.K., Coman, I.L., Radoeva, P.D., Bouix, S., Tang, Y., et al., 2016. Abnormalities in brain white matter in adolescents with 22q11.2 deletion syndrome and psychotic symptoms. Brain Imaging Behav. http://dx.doi.org/10.1007/s11682-016-9602-x.
Kikinis, Z., Makris, N., Finn, C.T., Bouix, S., Lucia, D., Coleman, M.J., et al., 2013. Genetic contributions to changes of fiber tracts of ventral visual stream in 22q11.2 deletion syndrome. Brain Imaging Behav. 7, 316–325.
Kljajevic, V., 2014. White matter architecture of the language network. Transl. Neurosci. 5, 239–252.
Li, F., Huang, X., Tang, W., Yang, Y., Li, B., Kemp, G.J., et al., 2014. Multivariate Pattern Analysis of DTI Reveals Differential White Matter in Individuals With Obsessive-compulsive Disorder. 35. pp. 2643–2651.
Ludwig, E., Klingler, J., 1956. Atlas cerebri humani. Der innere Bau des Gehirns dargestellt auf Grund makroskopischer Präparate./The Inner Structure of the Brain Demonstrated on the Macroscopical Preparations. Little, Brown, Boston.
Makris, N., 1999. Doctoral Thesis: Delineation of Human Association Fiber Pathways Using Histologic and Magnetic Resonance Methodologies.
Makris, N., Kennedy, D.N., McInerney, S., Sorensen, A.G., Wang, R., Caviness, V.S., et al., 2005. Segmentation of subcomponents within the superior longitudinal fascicle in humans: a quantitative, in vivo, DT-MRI study. Cereb. Cortex 15, 854–869.
Makris, N., Meyer, J.W., Bates, J.F., Yeterian, E.H., Kennedy, D.N., Caviness, V.S., 1999. MRI-based topographic parcellation of human cerebral white matter and nuclei. NeuroImage 9, 18–45.
Makris, N., Pandya, D.N., 2009. The extreme capsule in humans and rethinking of the language circuitry. Brain Struct. Funct. 213, 343–358.
Makris, N., Papadimitriou, G.M., Kaiser, J.R., Sorg, S., Kennedy, D.N., Pandya, D.N., 2009. Delineation of the middle longitudinal fascicle in humans: a quantitative, in vivo, DT-MRI study. Cereb. Cortex 19, 777–785.
Makris, N., Preti, M.G., Asami, T., Pelavin, P., Campbell, B., Papadimitriou, G.M., et al., 2013a. Human middle longitudinal fascicle: variations in patterns of anatomical connections. Brain Struct. Funct. 218, 951–968.
Makris, N., Preti, M.G., Wassermann, D., Rathi, Y., Papadimitriou, G.M., Yergatian, C., et al., 2013b. Human middle longitudinal fascicle: segregation and behavioral-clinical implications of two distinct fiber connections linking temporal pole and superior temporal gyrus with the angular gyrus or superior parietal lobule using multi-tensor tractography. Brain Imaging Behav. 7, 335–352.
Makris, N., Worth, A.J., Papadimitriou, G.M., Stakes, J.W., Caviness, V.S., Kennedy, D.N., et al., 1997. Morphometry of in vivo human white matter association pathways with diffusion-weighted magnetic resonance imaging. Ann. Neurol. 42, 951–962.
Makris, N., Zhu, A., Papadimitriou, G.M., Mouradian, P., Ng, I., Scaccianoce, E., et al., 2016. Mapping temporo-parietal and temporo-occipital cortico-cortical connections of the human middle longitudinal fascicle in subject-specific, probabilistic, and stereotaxic Talairach spaces. Brain Imaging Behav. 1–20. http://dx.doi.org/10.1007/s11682-016-9589-3.
Malcolm, J.G., Michailovich, O., Bouix, S., Westin, C.-F., Shenton, M.E., Rathi, Y., 2010a. A filtered approach to neural tractography using the Watson directional function. Med. Image Anal. 14, 58–69.
Malcolm, J.G., Shenton, M.E., Rathi, Y., 2010b. Filtered Multitensor Tractography. IEEE Trans. Med. Imaging 29, 1664–1675.
Maldonado, I.L., de Champfleur, N.M., Velut, S., Destrieux, C., Zemmoura, I., Duffau, H., 2013. Evidence of a middle longitudinal fasciculus in the human brain from fiber dissection. J. Anat. 223, 38–45.
McCabe, K.L., Marlin, S., Cooper, G., Morris, R., Schall, U., Murphy, D.G., et al., 2016. Visual perception and processing in children with 22q11.2 deletion syndrome: associations with social cognition measures of face identity and emotion recognition. J. Neurodev. Disord. 8, 30.
Menjot de Champfleur, N., Lima Maldonado, I., Moritz-Gasser, S., Machi, P., Le, Bars E., Bonafé, A., et al., 2013. Middle longitudinal fasciculus delineation within language pathways: a diffusion tensor imaging study in human. Eur. J. Radiol. 82, 151–157.
Mesulam, M.M., Thompson, C.K., Weintraub, S., Rogalski, E.J., 2015. The Wernicke conundrum and the anatomy of language comprehension in primary progressive aphasia. Brain 138, 2423–2437.
Meyer, D., Dimitriadou, E., Hornik, K., Weingessel, A., Leisch, F., Chang, C.-C., et al., 2015. e1071: Misc Functions of the Department of Statistics, Probability Theory Group. at. https://cran.r-project.org/web/packages/e1071/index.html.
Miller, T.J., Mcqlashan, T.H., Rosen, J.L., Cadenhead, K., Ventura, J., Mcfarlane, W., et al., 2003. Prodromal assessment with the Structured Interview for prodromal Syndromes and the scale of prodromal symptoms: predictive validity, interrater reliability, and training to reliability. Schizophr. Bull. 29, 703–715.
Murphy, K.C., Jones, L.A., Owen, M.J., 1999. High rates of schizophrenia in adults with velo-cardio-facial syndrome. Arch. Gen. Psychiatry 56, 940–945.
O'Dwyer, L., Lamberton, F., Bokde, A.L.W., Ewers, M., Faluyi, Y.O., Tanner, C., et al., 2012. Using Support Vector Machines With Multiple Indices of Diffusion for Automated Classification of Mild Cognitive Impairment. pp. 7.
Orrù, G., Pettersson-Yeo, W., Marquand, A.F., Sartori, G., Mechelli, A., 2012. Using support vector machine to identify imaging biomarkers of neurological and psychiatric disease: a critical review. Neurosci. Biobehav. Rev. 36, 1140–1152.
Ottet, M.C., Schaer, M., Cammoun, L., Schneider, M., Debbané, M., Thiran, J.P., et al., 2013. Reduced fronto-temporal and limbic connectivity in the 22q11.2 deletion syndrome: vulnerability markers for developing schizophrenia? PLoS One 8.
Pandya, D., Petrides, M., Cipolloni, P.B., 2015. Cerebral Cortex: Architecture,

Connections, and the Dual Origin Concept. Oxford University Press, New York, NY.
Perlstein, M.D., Chohan, M.R., Coman, I.L., Antshel, K.M., Fremont, W.P., Gnirke, M.H., et al., 2014. White matter abnormalities in 22q11.2 deletion syndrome: preliminary associations with the Nogo-66 receptor gene and symptoms of psychosis. Schizophr. Res. 152, 117–123.
Peruzzo, D., Castellani, U., Perlini, C., Bellani, M., Marinelli, V., Rambaldelli, G., et al., 2015. Classification of first-episode psychosis: a multi-modal multi-feature approach integrating structural and diffusion imaging. 122. pp. 897–905.
Pettersson-Yeo, W., Benetti, S., Marquand, A.F., Dell'Acqua, F., Williams, S.C.R., Allen, P., et al., 2013. Using Genetic, Cognitive and Multi-modal Neuroimaging Data to Identify Ultra-high-risk and First-episode Psychosis at the Individual Level. 43. pp. 2547–2562.
Phillips, O.R., Nuechterlein, K.H., Clark, K.A., Hamilton, L.S., Asarnow, R.F., Hageman, N.S., et al., 2009. Fiber tractography reveals disruption of temporal lobe white matter tracts in schizophrenia. Schizophr. Res. 107, 30–38.
Quinn, T., Tylee, D., Glatt, S., Quinn, T., Tylee, D., Glatt, S., 2016. Exprso: An R-package for the Rapid Implementation of Machine Learning Algorithms. 5. F1000Researchpp. 2588.
Radoeva, P.D., Coman, I.L., Antshel, K.M., Fremont, W., McCarthy, C.S., Kotkar, A., et al., 2012. Atlas-based white matter analysis in individuals with velo-cardio-facial syndrome (22q11.2 deletion syndrome) and unaffected siblings. Behav. Brain Funct. 8, 38.
Rathi, Y., Kubicki, M., Bouix, S., Westin, C.-F., Goldstein, J., Seidman, L., et al., 2011. Statistical analysis of fiber bundles using multi-tensor tractography: application to first-episode schizophrenia. Magn. Reson. Imaging 29, 507–515.
Ritchie, M.E., Phipson, B., Wu, D., Hu, Y., Law, C.W., Shi, W., et al., 2015. Limma powers differential expression analyses for RNA-sequencing and microarray studies. Nucleic Acids Res, gkv007. http://dx.doi.org/10.1093/nar/gkv007.
Saur, D., Kreher, B.W., Schnell, S., Kümmerer, D., Kellmeyer, P., Vry, M.-S., et al., 2008. Ventral and dorsal pathways for language. Proc. Natl. Acad. Sci. U. S. A. 105, 18035–18040.
Scariati, E., Padula, M.C., Schaer, M., Eliez, S., 2016. Long-range dysconnectivity in frontal and midline structures is associated to psychosis in 22q11.2 deletion syndrome. J. Neural Transm. 123, 823–839.
Schmahmann, J.D., Pandya, D.N., 2006. Fiber Pathways of the Brain. Oxford University Press, New York, NY.
Schmahmann, J.D., Pandya, D.N., Wang, R., Dai, G., D'Arceuil, H.E., De Crespigny, A.J., et al., 2007. Association fibre pathways of the brain: parallel observations from diffusion spectrum imaging and autoradiography. Brain 130, 630–653.
Schneider, M., Debbané, M., Bassett, A.S., Chow, E.W.C., Fung, W.L.A., van den Bree, M.B.M., et al., 2014. Psychiatric disorders from childhood to adulthood in 22q11.2 deletion syndrome: results from the international consortium on brain and behavior in 22q11.2 deletion syndrome. Am. J. Psychiatry 171, 627–639.
de Schotten, M.T., Dell'Acqua, F., Forkel, S.J., Simmons, A., Vergani, F., Murphy, D.G.M., et al., 2011. A lateralized brain network for visuospatial attention. Nat. Neurosci. 14, 1245–1246.
Seitz, J., Zuo, J.X., Lyall, A.E., Makris, N., Kikinis, Z., Bouix, S., et al., 2016. Tractography analysis of 5 white matter bundles and their clinical and cognitive correlates in early-course schizophrenia. Schizophr. Bull. 42, 762–771.
Seltzer, B., Pandya, D.N., 1984. Further observations on parieto-temporal connections in the rhesus monkey. Exp. Brain Res. 55, 301–312.
Da Silva Alves, F., Schmitz, N., Bloemen, O., van der Meer, J., Meijer, J., Boot, E., et al., 2011. White matter abnormalities in adults with 22q11 deletion syndrome with and without schizophrenia. Schizophr. Res. 132, 75–83.
Simon, T.J., Bearden, C.E., Moss, E.M., McDonald-McGinn, D., Zackai, E., Wang, P.P., 2002. Cognitive development in VCFS. Prog. Pediatr. Cardiol. 15, 109–117.
Simon, T.J., Ding, L., Bish, J.P., McDonald-McGinn, D.M., Zackai, E.H., Gee, J., 2005. Volumetric, connective, and morphologic changes in the brains of children with chromosome 22q11.2 deletion syndrome: an integrative study. NeuroImage 25, 169–180.
Simon, T.J., Wu, Z., Avants, B., Zhang, H., Gee, J.C., Stebbins, G.T., 2008. Atypical cortical connectivity and visuospatial cognitive impairments are related in children with chromosome 22q11.2 deletion syndrome. Behav. Brain Funct. 4, 25.
Smith, S.M., Jenkinson, M., Woolrich, M.W., Beckmann, C.F., Behrens, T.E.J., Johansen-Berg, H., Bannister, P.R., De Luca, M., Drobnjak, I., Flitney, D.E., Niazy, R.K., Saunders, J., Vickers, J., Zhang, Y., De Stefano, N., Brady, J.M., Matthews, P.M., 2004. Advances in functional and structural MR image analysis and implementation as FSL. NeuroImage 23, S208–S219.
Song, S.K., Yoshino, J., Le, T.Q., Lin, S.J., Sun, S.W., Cross, A.H., et al., 2005. Demyelination increases radial diffusivity in corpus callosum of mouse brain. NeuroImage 26, 132–140.
Sundram, F., Campbell, L.E., Azuma, R., Daly, E., Bloemen, O.J.N., Barker, G.J., et al., 2010. White matter microstructure in 22q11 deletion syndrome: a pilot diffusion tensor imaging and voxel-based morphometry study of children and adolescents. J. Neurodev. Disord. 2, 77–92.
Swillen, A., Devriendt, K., Legius, E., Eyskens, B., Dumoulin, M., Gewillig, M., et al., 1997. Intelligence and psychosocial adjustment in velo-cardio-facial syndrome: a study of 37 children and adolescents with VCFS. Genet. Couns. 8, 260–261.
Tan, G.M., Arnone, D., McIntosh, A.M., Ebmeier, K.P., 2009. Meta-analysis of magnetic resonance imaging studies in chromosome 22q11.2 deletion syndrome (velocardiofacial syndrome). Schizophr. Res. 115, 173–181.
Váša, F., Griffa, A., Scariati, E., Schaer, M., Urben, S., Eliez, S., et al., 2016. An affected core drives network integration deficits of the structural connectome in 22q11.2 deletion syndrome. NeuroImage Clin. 10, 239–249.
Villalon-Reina, J., Jahanshad, N., Beaton, E., Toga, A.W., Thompson, P.M., Simon, T.J., 2013. White matter microstructural abnormalities in girls with chromosome 22q11.2 deletion syndrome, Fragile X or Turner syndrome as evidenced by diffusion tensor imaging. NeuroImage 81, 441–454.
Di Virgilio, G., Clarke, S., 1997. Direct interhemispheric visual input to human speech areas. Hum. Brain Mapp. 5, 347–354.
Wang, Y., Fernandez-Miranda, J.C., Verstynen, T., Pathak, S., Schneider, W., Yeh, F.-C., 2013. Rethinking the role of the middle longitudinal fascicle in language and auditory pathways. Cereb. Cortex 23, 2347–2356.
Wassermann, D., Makris, N., Rathi, Y., Shenton, M., Kikinis, R., Kubicki, M., et al., 2013. On Describing Human White Matter Anatomy: The White Matter Query Language. Lect Notes Comput Sci (Including Subser Lect Notes Artif Intell Lect Notes Bioinformatics). 8149. LNCSpp. 647–654.
Wassermann, D., Makris, N., Rathi, Y., Shenton, M., Kikinis, R., Kubicki, M., et al., 2016. The white matter query language: a novel approach for describing human white matter anatomy. Brain Struct. Funct. 221, 4705–4721.
Wechsler, D., 1997. Wechsler Adult Intelligence Scale (Third Ed.).